Casting of Gold Nanoparticles with High Aspect Ratios inside DNA Molds

Jingjing Ye, Richard Weichelt, Ulrich Kemper, Vaibhav Gupta, Tobias A. F. König, Alexander Eychmüller, and Ralf Seidel*

DNA nanostructures provide a powerful platform for the programmable assembly of nanomaterials. Here this approach is extended to synthesize rod-like gold nanoparticles in a full DNA controlled manner. The approach is based on DNA molds containing elongated cavities. Gold is deposited inside the molds using a seeded-growth procedure. By carefully exploring the growth parameters it is shown that gold nanostructures with aspect ratios of up to 7 can be grown from single seeds. The highly anisotropic growth is in this case controlled only by the rather soft and porous DNA walls. The optimized seeded growth procedure provides a robust and simple routine to achieve continuous gold nanostructures using DNA templating.

1. Introduction

In the past decades, researchers have utilized the unique programmable base-pairing of DNA for the construction of artificial soft matter structures. Since the first demonstration of the assembly of a DNA junction by Ned Seeman,[1] structural DNA nanotechnology has developed into a rapidly advancing field that allows to design and fabricate complex 2D and 3D nucleic acid structures with nanometer precision.[2–4] While being powerful

Dr. J. Ye, Dr. R. Weichelt, U. Kemper, Prof. R. Seidel
Molecular Biophysics group
Peter Debye Institute for Soft Matter Physics
Universität Leipzig
Leipzig 04103, Germany
E-mail: ralf.seidel@physik.uni-leipzig.de
Dr. J. Ye, Dr. R. Weichelt, U. Kemper, Prof. R. Seidel
Center for Advancing Electronics Dresden
Technische Universität Dresden
Dresden 01062, Germany
Dr. R. Weichelt, Prof. A. Eychmüller
Physical Chemistry and Center for Advancing Electronics Dresden
Technische Universität Dresden
Dresden 01062, Germany
V. Gupta, Dr. T. A. F. König
Institute for Physical Chemistry and Polymer Physics
Leibniz-Institut für Polymerforschung Dresden
e.V., Hohe Str. 6, Dresden 01069, Germany

in assembling soft objects, the DNA-based fabrication of "hard matter" structures comprising metals or semiconductors, for example, for nanoelectronic and nano-optic applications remains challenging. The most commonly applied method is a site-specific attachment of preformed nanoparticles on DNA nanostructures in order to establish defined arrangements of individual particles.[5–9] An alternative approach that allows to form more continuous structures is the direct growth of the desired materials on a DNA template. This typically includes an initial attachment of nucleation seeds on the DNA structure. Subsequently, material deposition is catalyzed from the seeds (e.g., using electroless plating) in which the DNA template guides the shape of the resulting object.[10–16] A remaining problem of this approach is, however, the limited homogeneity of the fabricated material films, since the competing growth from the individual particles is difficult to control. Recently, we and others overcame part of these difficulties by using DNA origami structures as molds.[17,18] The metal deposition was catalyzed by a single gold nanoparticle (AuNP) seed inside the cavities of these structures, such that the shape of the resulting nanoparticle was to some extent determined and controlled by the mold walls. This way, particles that were slightly elongated along the axis of the mold cavity with maximum aspect ratios of 1:2 could be fabricated. This was considerably lower than obtained for mold-free gold nanorods synthesis schemes that use silver ions and surfactants to achieve a preferred growth along a given crystallographic direction.[19] In the mold approach, the aspect ratio was mainly limited by the fact that the material growth in transversal direction to the cavity axis was not sufficiently suppressed by the DNA walls.[17,20] This procedure could nonetheless be applied to fabricate μm-long gold nanowires with 20–30 nm diameter, by coupling individual seed-loaded tubular molds to long linear superstructures.[20] Wires with metallic conductivity could be obtained, however, their yield was limited by some remaining gaps between the many individually grown nanoparticles. These problems could be avoided, if the molds would support a true continuous "casting" of gold into the cavity that would originate from a single or few seeds only.
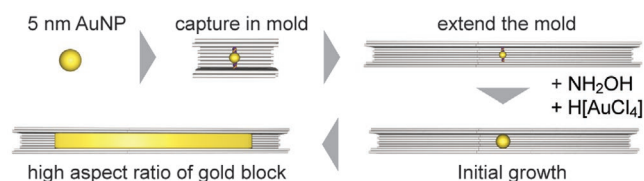
Here, we present an improved method for the metal deposition inside DNA origami-based molds that fosters a highly anisotropic growth of gold nanoparticles from single AuNP seeds (**Figure 1**). In turn, this allows to form wire structures using a greatly reduced number of AuNPs. Key for the development of

ADVANCED
SCIENCE NEWS
www.advancedsciencenews.com

NANO · MICRO
small
www.small-journal.com

Figure 1. Assembly scheme for the fabrication of rod-like nanoparticles with high aspect ratios. DNA origami molds are loaded with single 5 nm AuNP seeds, followed by the docking of additional molds at the mold termini. A seeded gold growth procedure allows particle growth, which shall optimally adopt the shape of the mold cavity such that anisotropic gold nanorods are obtained.

an optimized methodology was a careful scanning of various reaction parameters to gain better control over the gold growth conditions and the associated reaction kinetics.
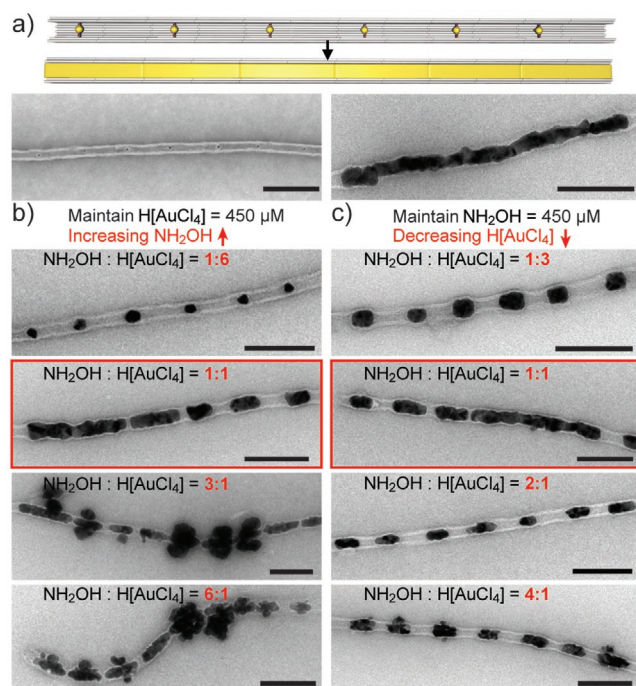
2. Results

The setup for testing different growth conditions was based on μm-long linear mold superstructures. These were assembled from DNA origami monomers of quadratic cross-section.[20] Their outer dimension was formed by a 10×10 DNA helix array of 40 nm length. The mold walls were formed by a double layer of DNA helices providing an edge length of the inner cavity of ≈17 nm. Two different types of mold monomers were prepared possessing specific, mutually attractive ends. Molds of one type

Figure 2. a) Scheme of the gold casting procedure using linear mold superstructures with AuNP seeds in every second mold monomer (top) and TEM images of a superstructure before and after casting with optimized conditions (bottom). b) Testing increasing amounts of reducing agent for a fixed gold precursor concentration of 450 μM. c) Testing decreasing amounts of gold precursor for a fixed concentration of reducing agent of 450 μM. The scale bar in all TEM images corresponds to 100 nm.

were decorated with single AuNP seeds in their centers. Mixing both types of monomers resulted in the formation of long periodic chains of the two mold types (**Figure 2**a), such that only every second mold was decorated with an AuNP seed. This provided interparticle distances of 80 nm that were sufficiently large to test anisotropic particle growth that would be imposed by the mold walls along the mold axis.

The previously applied seeded growth procedure for metal deposition inside DNA molds uses a mixture of the gold precursor $HAuCl_4$ and the reducing agent NH_2OH. In absence of suitable nuclei this solution is stable (Figure S1, Supporting Information). Gold reduction is, however, catalyzed when adding the seed-loaded mold structures (at a final seed concentration of 0.5 nM), such that gold growth inside the mold cavity occurs (Figure 2a). We first tested how the molar ratio between the two reagents influenced the shape of the grown particles. We initially kept the total concentration of chloroauric acid constant and investigated increasing amounts of hydroxylamine (Figure 2b) covering molar ratios between NH_2OH and $HAuCl_4$ from 1:6 to 6:1. At the lowest concentration of reducing agent (1:6) at which presumable not all chloroauric acid was reduced, spherical AuNP with diameters of 15 ± 2 nm ($N = 25$) were obtained (Figure 2b). Larger particles started to expand the mold sidewalls confirming the elasticity of DNA molds.[18] Doubling the concentration of the reducing agent led to far more elongated cuboid-shaped particles that partially started to merge to each other. The average length of single particles was 46 ± 10 nm, while the particle diameters were 18 ± 2 nm, providing aspect ratios of ≈2.5 ($N = 20$) for the single particles. A highly anisotropic gold growth was also achieved for NH_2OH: $HAuCl_4$ ratios of 1:1.5, 1:1, and 1.5:1, respectively (Figure 2b and Figure S2a, Supporting Information). For the 1:1 ratio, the mean length of single (isolated) particles was 62 ± 13 nm. Given a mean particle diameter of 21 ± 3 nm, aspect ratios of 2.9 ($N = 20$) were obtained. At high molar ratios between NH_2OH and $HAuCl_4$ of 3:1 and 6:1 at which all gold precursor should have reacted, an anisotropic growth was still observable albeit at a reduced extent. Additionally, gold deposition at the outside of the mold was frequently observed (Figure 2b). The TEM images suggested that the internal gold growth could leak through the walls, presumably at damage points of the DNA structure mold. The occurrence of such a "leaky" growth that can bypass smaller cavities within the mold walls, indicated that the metal growth might include the formation of smaller grains and extrusions at the surface of the growing particle which may enter the cavities. Altogether, a molar ratio between gold precursor and reducing agent around 1:1 provided the highest anisotropy for the gold particles.

To fine-tune the reaction conditions, we next kept the concentration of the reducing agent constant at 450 μM and varied the gold precursor concentration between molar NH_2OH: $HAuCl_4$ ratios of 1:3 to 4:1 (Figure 2c and Figure S2b, Supporting Information). At the lowest molar ratio of 1:3, the AuNPs had again a spherical shape (compare Figure 2b,c). Due to their large sizes, the elastic mold sidewalls became heavily expanded without resulting in a leaky growth. As before, anisotropic but leaky growth was observed for the highest molar ratio of 4:1. This is remarkable, since in this case much less gold precursor was applied compared to the experiments with constant concentration of reducing agent. Again, a ≈1:1 ratio between NH_2OH

ADVANCED
SCIENCE NEWS
www.advancedsciencenews.com

NANO · MICRO
small
www.small-journal.com

and HAuCl$_4$ provided the best anisotropic particle growth and the most frequent formation of continuous wire-like sections (Figure 2c). The 1:1 ratio seemed to best balance between a too homogeneous growth (low NH$_2$OH : HAuCl$_4$ ratios) and a too anisotropic growth where even fine mold details, such as wall cavities, became filled (leakage at high NH$_2$OH : HAuCl$_4$ ratios). Therefore, a 1:1 ratio was applied for all subsequent experiments. We also tested different orders in which the reactants were mixed, without finding a significant difference (Figure S3, Supporting Information).

In contrast to typical electroless plating solutions, the mold-based gold growth requires the presence of magnesium ions to support the stability of the DNA origami structures. Furthermore, sodium ions are typically present from the loading step of the AuNP seeds into the molds. We therefore tested how the gold growth is influenced by the ionic strength of the solution in particular concentrations of sodium chloride (NaCl) of 0, 20, 60, and 100 mM. To this end sodium ions were first removed from the seed-loaded mold solution using polyethylene glycol (PEG) purification followed by addition of the desired amount of NaCl. The concentrations of precursor and reducing agent were kept constant at 450 µM. In absence of NaCl, anisotropic gold nanoparticles with lengths between 62 ± 10 nm and widths of 21 ± 2 nm (N = 15) were formed (**Figure 3**a, Figure S6, Supporting Information). In contrast, addition of NaCl facilitated an isotropic growth of the AuNPs. At 20 mM NaCl, the particle width was reduced to 18 ± 3 nm and the average length shortened to 37 ± 5 nm (N = 25). The strong reduction of the aspect ratio was even more pronounced for 60 and 100 mM of NaCl, where most of the grown AuNPs were of spherical and some fraction of particles of triangular shape. In this case, the average AuNP diameter increased again to 23 ± 2 (N = 20) and 21 ± 2 nm (N = 15), respectively, which led to a noticeable local expansion of the mold sidewalls (see, e.g., Figure 3a, lower left).
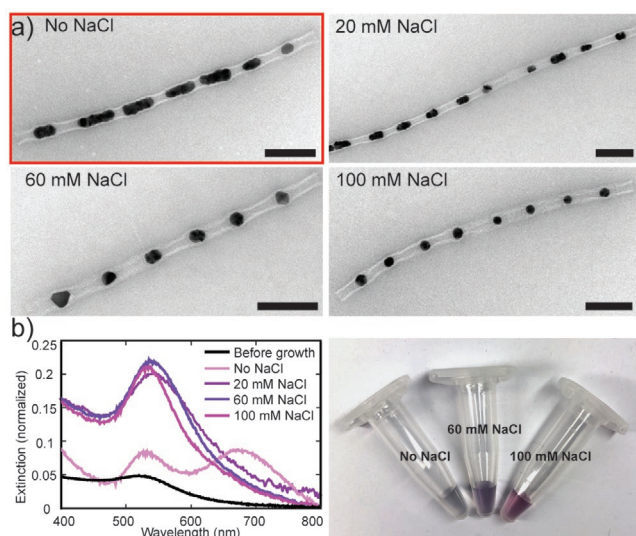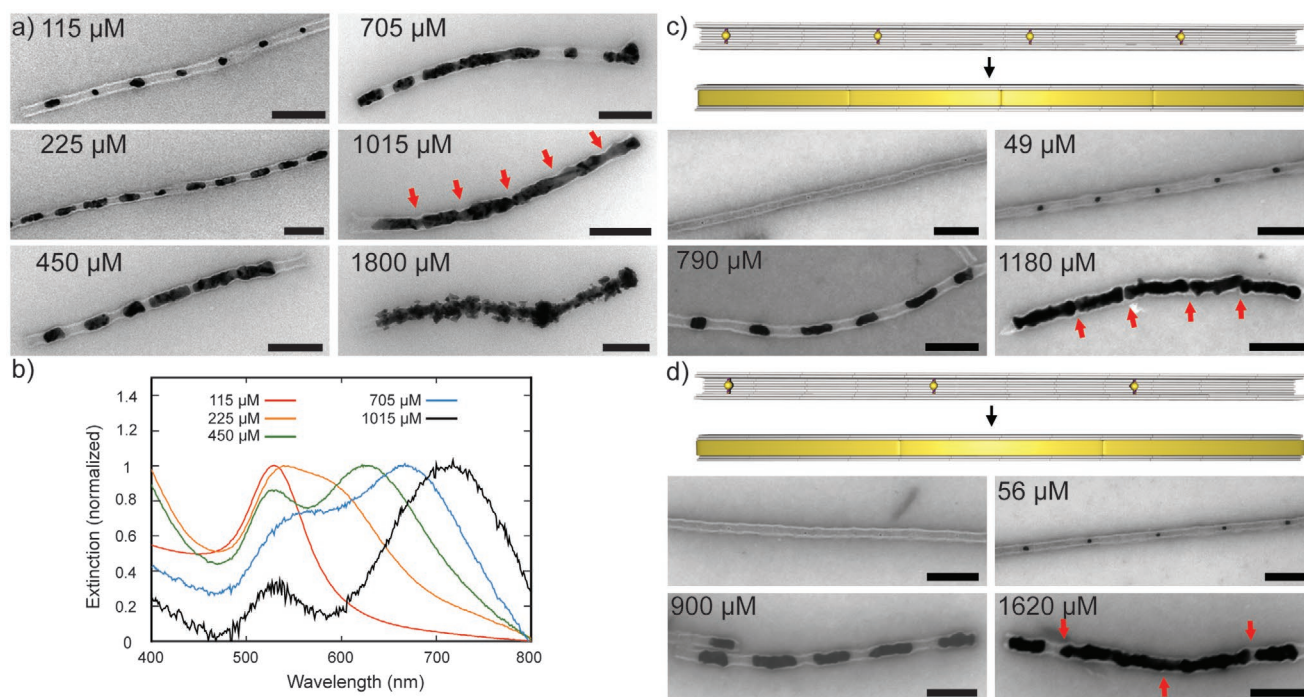
Similar results were obtained for gold particles grown in specific mold trimer structures at different NaCl concentrations (Figure S4, Supporting Information).

The influence of NaCl on the shape of the nanoparticles was also apparent in different colors of the obtained particle solutions (Figure 3b). We recorded extinction spectra for the initially present 5 nm AuNPs as well as the grown particles at 0, 20, 60, and 100 mM NaCl immediately after the reaction was completed (Figure 3b). The 5 nm AuNPs seeds exhibited an extinction maximum at 521 nm (Figure 3b) which is due to the excitation of the localized surface plasmon resonance in these spherical particles.[21] For the anisotropic particles grown in absence of NaCl, two extinction maxima at 531 nm and at 674 nm became apparent, which can be attributed to electric field excitation along the short (transversal mode) and long axes (longitudinal mode) of the particles, respectively.[21,22] The geometry of the particles is related to these plasmonic modes, from which one can also conclude the aspect ratio. The maxima of the transverse mode shifted from 521 nm measured for the 5 nm AuNPs to 531 nm, due to the increased diameter of the rods. The spectra for the particles grown at 60 and 100 mM NaCl did not exhibit a separate longitudinal mode, which is in agreement with the spherical shape of the AuNPs. The local extinction maximum shifted to 538 and 536 nm, for 60 and 100 mM NaCl, respectively, which is larger than expected given the diameters of the particles inside the molds. We attribute the moderate shift to the presence of larger AuNPs that were observed in wide-field TEM images only in these particle preparations (Figure S5, Supporting Information). From the synthesis point of view, we think that they originate from free residual AuNPs seeds. As reported previously, elevated ionic strengths reduce the electrostatic repulsion and promote the aggregation of small particles to larger ones.[23] These particles are then rapidly growing at the expense of the small AuNPs inside of the molds, which also explains the poor filling of the molds at elevated NaCl concentrations.

We next tested different levels of gold deposition inside the mold chains (**Figure 4**a). To this end, equal concentrations of gold precursor and reducing agent between 115 and 1800 µM were applied. At the lowest concentration, spherical and slightly elongated AuNPs with a width of 14 ± 2 nm and a length of 23 ± 8 nm (N = 15) were obtained. The extinction spectrum showed a single plasmonic mode at 528 nm (Figure 4b). For 225 µM, the spectrum displayed an additional shoulder around 579 nm indicating a distinct longitudinal plasmonic mode in agreement with an anisotropic shape of the particles with an aspect ratio of 2.8 (N = 20) observed by TEM imaging. Increasing concentrations of gold precursor and reducing agent provided correspondingly larger aspect ratios (Figure 4a, Figure S7, Supporting Information). This trend was confirmed by measured extinction spectra, where the longitudinal plasmonic mode was increasingly red-shifted, while the position of the transversal plasmonic mode remained approximately constant (Figure 4b, Figure S7a, Supporting Information). In addition, the longitudinal mode became increasingly prominent. These observations were in qualitative agreement with extinction spectra from theoretical simulations (Figure S8, Supporting Information). The larger spectral width of the longitudinal mode in the measurements was attributed to the existing spread of particle lengths. With increasing precursor

Figure 3. a) Gold growth inside mold superstructures for different concentrations of NaCl using a 1:1 ratio of HAuCl$_4$: NH$_2$OH. b) Extinction spectra of the structures shown in a before and after growth at varying NaCl concentrations. AuNPs. Scale bar in all TEM images is 100 nm. Photographic image of the different solutions after gold growth.

Figure 4. a) TEM images of mold superstructures after gold growth for increasing stoichiometric amounts of gold precursor and reducing agent. b) Extinction spectra recorded for the samples shown in (a). c) Scheme and TEM images of mold chains with 120 nm distance between two AuNPs before and after gold deposition at the indicated concentrations of precursor and reducing agent. d) Scheme and TEM images of mold chains with 160 nm distance between two AuNPs before and after gold deposition. Scale bar in all images is 100 nm.

concentration an increasing fraction of particles merged with their neighbors. The diameters of such wire-like sections of 20 ± 2 nm were found to be rather homogenous. Inside these sections the single particle length reached 80 ± 11 nm ($N = 20$) at 1015 µM gold precursor concentration yielding an aspect ratio of 4.0. For even higher gold precursor concentrations (1800 µM), aggregates formed during the synthesis that deposited on the bottom of the reaction vessel. TEM imaging revealed that the gold growth was leaky in this case (Figure 4b). This suggested that the additionally added gold could not be accommodated anymore by the elastic expansion of the mold walls.

To explore the limits of the anisotropic particle growth within DNA molds, we assembled linear mold superstructures where a seed-loaded monomer was introduced only at every third and every fourth position.[24] The distance between neighboring AuNP seeds was thus increased to 120 and 160 nm (see Figure 4c,d, respectively). These mold structures were subsequently subjected to the gold growth procedure using three different gold precursor concentrations. For the molds with 120 nm seed spacing, the particle aspect ratios increased from 1.0 to 2.6 and finally to 5.0 for precursor concentrations of 49, 790, and 1180 µM, respectively (Figure 4c, Figure S9c, Supporting Information). Correspondingly, the single particle length increased from 7 ± 1 nm ($N = 25$) to 53 ± 10 nm ($N = 20$) and to 105 ± 12 nm ($N = 20$). At 1180 µM gold precursor, the particles were almost completely connected to each other thus bridging the 120 nm inter-particle gap. At even higher concentrations, leaky growth and aggregation of the structures was observed (Figure S9a, Supporting Information). For the molds with 160 nm seed spacing, the particle aspect ratios increased from 1 to 3.8 to 6.8 for precursor concentrations of 56,

900, and 1620 µM, respectively (Figure 4d) with corresponding particle lengths of 8 ± 1 nm ($N = 25$), 72 ± 8 nm ($N = 20$), and 137 ± 11 nm ($N = 20$). At the highest gold precursor concentration, the particles were also in this case frequently connected, that is, a mold-guided particle growth over 160 nm could be achieved.

Finally, we tested whether our optimized seeded growth procedure can be applied to more complex mold geometries, which can be used to fabricate gold nanostructures with increased complexity. As an example we chose a branched T-shaped mold superstructure, which would allow to introduce junctions into linear nanowire geometries. Incorporating only two seeds in such a T-shaped element successfully allowed to fill the structure in which the gold growth expanded into three different directions (Figure S8, Supporting Information).

3. Discussion

In summary, we successfully established a seeded growth procedure for gold nanoparticles in which the growth can be guided over large length scales by the rather soft walls of the DNA mold structures. Using linear molds this supported the fabrication of highly anisotropic gold rods from single AuNP seeds. The reached aspect ratios of up to ≈7 corresponding to a length of ≈140 nm at ≈20 nm diameter exceeded previously obtained results significantly.[17,18] Thus, our method supported much better a "true casting" of gold into DNA molds. The reduced number of inter-particle contacts could provide higher yields of mold-templated gold nanowires with metallic conductivity which needs to be tested in future experiments. In contrast to template

free AuNP synthesis schemes,[19] the shape of the resulting particles can be rather freely dictated by correspondingly designed molds without developing a new synthesis procedure.[24]

Key of the developed procedure was a careful tuning of the reactant concentrations. An excess of gold precursor over reducing agent provided spherical particles with low anisotropy that significantly expanded the mold walls without becoming elongated (Figure 2b,c). In contrast, an excess of reducing agent over gold precursor provided anisotropic particles with less mold expansion but leaky growth through cavities in the mold walls. Only at equal stoichiometries between the two reagents anisotropic particle growth with largely suppressed leaky growth was obtained. Furthermore, addition of NaCl could shift the obtained morphologies towards spherical particles with low anisotropies. It has been previously shown that increasing concentrations of reducing agent allowed for the growth of thermodynamically less stable, that is, more anisotropic, particle morphologies due to an accelerated kinetics of the reduction process.[25] Addition of halides—in particular Br$^-$ and I$^-$—was in contrast providing thermodynamically more stable particle surfaces. This could be attributed to a decrease of the reduction potential of the gold ion species and the passivation of the gold nanoparticle surface.[25] Both effects slowed down the reaction kinetics in the order Cl$^-$ > Br$^-$ > I$^-$. A slow reaction kinetics as found at low $NH_2OH : HAuCl_4$ ratios and potentially at more elevated NaCl concentrations may thus explain the preference of spherical particles at these conditions. The particle shape in our experiments was, however, little dependent on the overall concentration of the reactants (compare Figure 2b,c), which disagrees with a pure kinetic mechanism for the shape control. Detailed analysis of the seeded growth of uniform spherical nanoparticles from platinum and gold has shown that the growth initiates via secondary nucleation leading to the formation of smaller nanometer-sized particles at the seed surface.[26,27] These particles grow and merge such that blackberry-like morphologies are obtained. In case of gold particles that have weaker metal bonds than platinum, smooth particle surfaces can be obtained in a subsequent ripening step at 100 °C. Interestingly, such an atomic reorganization is also obtained at room temperature when only 5 mM chloride ions are supplemented.[28] Most likely, chloride ion binding to the gold surface atoms lowers the binding energy and promotes the mobility of gold surface atoms during the ripening. This in turn allows the particles to adopt the thermodynamically preferred spherical conformation. Adopting this argument for the mold-based particle growth, spherical particles would be indeed expected for the excess of chloride-bound gold atoms at low amounts of reducing agent as well as at elevated NaCl concentrations. The minimization of the surface in this case is then a strong driving force that cannot be sufficiently counter-balanced by the mold walls. In contrast, at an excess of reducing agent or limited numbers of chloride ions, a redistribution of gold surface atoms would be inhibited. In this case, smaller gold clusters become deposited at the accessible sites in the mold channel, such that anisotropic particle growth can occur. Likely, the fast kinetics at the highest concentrations of reducing agent support nucleation of very small clusters that can even fill small cavities inside the mold walls, such that leaky growth is facilitated. We think that such a tunable mobility of the gold surface atoms best explains the found optimum for anisotropic particle growth in DNA molds. In agreement with such a model, high resolution TEM images of the seeds, the spherical particles at elevated NaCl (Figure S11, Supporting Information) and the anisotropic particles (Figure S12, Supporting Information) show that they all have a polycrystalline structure. This supports the idea of secondary nucleation during the growth of both the spherical and the anisotropic particles, which is followed by a different extent of reorganization or ripening depending on the conditions. This model could be further tested alongside an optimization of our procedure by involving other halide ion species or silver ions together with single-crystalline seeds, thus potentially allowing for gold casting in even larger and more complex mold structures.

4. Experimental Section

DNA Origami Assembly: The DNA origami molds[29] were designed using CaDNAno,[30] comprising parallel helices arranged in a square lattice.[31] Design details of the linear mold superstructures with different periodicities were provided previously.[24] For the assembly of mold monomers, 10 nM single-stranded p8064 scaffold DNA (tilibit nanosystems, Garching, Germany) was mixed in folding buffer (5 mM Tris-HCl, 1 mM EDTA, and 11 mM MgCl$_2$ (pH 8.0)) with staple strands and AuNP capture strands (Eurofins) in a molar ratio of 1:10:1 (per individual sequence). The reaction was heated to 80 °C for 5 min, and cooled to 25 °C over 15 h using a non-linear temperature ramp with the slowest temperature decrease occurring between 55 and 45 °C. Subsequently, the molds were purified using precipitation with PEG to remove excess staples.[32]

Preparation of Mold Chain Structure with Loaded AuNP Seeds: 5 nm AuNPs (Sigma-Aldrich) were densely coated with 15 nt poly-thymidine oligonucleotides carrying a 5'-thiol modification using salt aging.[33,34] The final AuNP concentration was calculated from the absorbance signal at 520 nm. The ssDNA AuNPs were then mixed with DNA mold monomers at a molar ratio of 3:1 per seed binding site. The mixture was slowly heated to 40 °C and afterwards cooled down to 23 °C over the course of a 5 h time period. To form different mold chain patterns, the different mold monomers were mixed at equal stoichiometry in folding buffer supplemented with 350 mM NaCl and incubated overnight. The mold monomers carried mutually complementary interfaces to support the formation of chains with different periodicities as described before.[24] The final mold chain structures were purified from excess AuNPs using PEG precipitation.[32]

Seeded-Growth: The concentration of seed loaded mold chain structures was calculated from the DNA absorbance at 260 nm. It was adjusted such that the final concentration of AuNP seeds was 0.5 nM. The seeded-growth was performed in folding buffer solution. Hydroxyl amine (NH$_2$OH) was mixed with gold precursor (H[AuCl$_4$]) in a desired molar ratio (see main text) in folding buffer while stirring the solution. Different concentrations of gold precursor were used for different gold growth procedures, varying from 115 µM up to 1800 µM. Gold growth inside the molds was initiated by adding seed-loaded mold chain structures to the growth solution. During the growth the solution was vigorously stirred and after 2 min the grown structures were deposited on TEM grids. For TEM imaging, 2–3 µL of the solution were applied onto glow-discharged carbon-coated grids. The sample was subsequently stained using a filtered 2% solution of uranyl formate in 5 mM NaOH for 10 s. TEM imaging was performed using a JEOL JEM1400Plus transmission electron microscope at 120 kV or a Jeol JEM2100Plus transmission electron microscope at 200 kV. tSEM imaging was performed on a Gemini SEM500 scanning electron microscope (Zeiss) operated in transmission mode at 25 kV. Absorption spectra were recorded using a Cary 60 UV–vis spectrophotometer from Agilent Technologies.

Finite-Difference in Time Domain Simulations: A commercial-grade software package (Lumerical FDTD, version 8.16) was used to execute the finite-difference in time domain (FDTD) simulations. The geometry of the nanoparticle were consisting a cylinder with two hemispherical caps. The optical response was simulated using a plane wave source and the frequency points were set equal to that of the wavelength span. The data for dielectric properties of gold was taken from Johnson and Christy and was fitted using six coefficients with an rms error of 0.2. Perfectly matched layer boundary conditions were used to obtain the scattering and absorption cross section of the gold nanorods. A sweep of various rod lengths was performed in order to calculate the cross sections. Longitudinal and transversal modes were excited by keeping the source polarization parallel and perpendicular to the long axis of the nano-rod, respectively. The mesh size in the FDTD region was set to 1 nm over the nano-rod geometry. All simulation reached an auto shutoff of at least 10^{-7}. The overall mesh region was chosen to be at least 100 nm larger than the structure.

Supporting Information

Supporting Information is available from the Wiley Online Library or from the author.

Acknowledgements

Conflict of Interest

The authors declare no conflict of interest.

Keywords

[1] N. C. Seeman, *J. Theor. Biol.* **1982**, *99*, 237.
[2] A. A. Arora, C. de Silva, *Nano Rev. Exp.* **2018**, *9*, 1430976.
[3] D. Mathur, I. L. Medintz, *Anal. Chem.* **2017**, *89*, 2646.
[4] F. Hong, F. Zhang, Y. Liu, H. Yan, *Chem. Rev.* **2017**, *117*, 12584.
[5] Y. Ma, X. Yang, Y. Wei, Q. Yuan, *Chin. J. Chem.* **2016**, *34*, 291.
[6] N. Liu, T. Liedl, *Chem. Rev.* **2018**, *118*, 3032.
[7] X. Wang, C. Li, D. Niu, R. Sha, N. C. Seeman, J. W. Canary, *Nano Lett.* **2018**, *18*, 2112.
[8] R. Weichelt, J. Ye, U. Banin, A. Eychmüller, R. Seidel, *Chem. – Eur. J.* **2019**, *25*, 9012.
[9] A. Xu, J. N. Harb, M. A. Kostiainen, W. L. Hughes, A. T. Woolley, H. Liu, A. Gopinath, *MRS Bull.* **2017**, *42*, 943.
[10] B. Uprety, T. Westover, M. Stoddard, K. Brinkerhoff, J. Jensen, R. C. Davis, A. T. Woolley, J. N. Harb, *Langmuir* **2017**, *33*, 726.
[11] B. Teschome, S. Facsko, T. Schönherr, J. Kerbusch, A. Keller, A. Erbe, *Langmuir* **2016**, *32*, 10159.
[12] B. Uprety, E. P. Gates, Y. Geng, A. T. Woolley, J. N. Harb, *Langmuir* **2014**, *30*, 1134.
[13] Y. Geng, A. C. Pearson, E. P. Gates, B. Uprety, R. C. Davis, J. N. Harb, A. T. Woolley, *Langmuir* **2013**, *29*, 3482.
[14] A. C. Pearson, J. Liu, E. Pound, B. Uprety, A. T. Woolley, R. C. Davis, J. N. Harb, *J. Phys. Chem. B* **2012**, *116*, 10551.
[15] J. Liu, Y. Geng, E. Pound, S. Gyawali, J. R. Ashton, J. Hickey, A. T. Woolley, J. N. Harb, *ACS Nano* **2011**, *5*, 2240.
[16] A. Stern, G. Eidelshtein, R. Zhuravel, G. I. Livshits, D. Rotem, A. Kotlyar, D. Porath, *Adv. Mater.* **2018**, *30*, 1800433.
[17] S. Helmi, C. Ziegler, D. J. Kauert, R. Seidel, *Nano Lett.* **2014**, *14*, 6693.
[18] W. Sun, E. Boulais, Y. Hakobyan, W. L. Wang, A. Guan, M. Bathe, P. Yin, *Science* **2014**, *346*, 1258361.
[19] M. J. Schnepf, M. Mayer, C. Kuttner, M. Tebbe, D. Wolf, M. Dulle, T. Altantzis, P. Formanek, S. Förster, S. Bals, T. A. F. König, A. Fery, *Nanoscale* **2017**, *9*, 9376.
[20] T. Bayrak, S. Helmi, J. Ye, D. Kauert, J. Kelling, T. Schönherr, R. Weichelt, A. Erbe, R. Seidel, *Nano Lett.* **2018**, *18*, 2116.
[21] V. Amendola, R. Pilot, M. Frasconi, O. M. Maragò, M. A. Iatì, *J. Phys. Condens. Matter* **2017**, *29*, 203002.
[22] M. Karg, T. A. F. König, M. Retsch, C. Stelling, P. M. Reichstein, T. Honold, M. Thelakkat, A. Fery, *Mater. Today* **2015**, *18*, 185.
[23] L. Zhao, D. Jiang, Y. Cai, X. Ji, R. Xie, W. Yang, *Nanoscale* **2012**, *4*, 5071.
[24] J. Ye, S. Helmi, J. Teske, R. Seidel, *Nano Lett.* **2019**, *19*, 2707.
[25] M. R. Langille, M. L. Personick, J. Zhang, C. A. Mirkin, *J. Am. Chem. Soc.* **2012**, *134*, 14542.
[26] C. Ziegler, A. Eychmüller, *J. Phys. Chem. C* **2011**, *115*, 4502.
[27] N. C. Bigall, T. Härtling, M. Klose, P. Simon, L. M. Eng, A. Eychmüller, *Nano Lett.* **2008**, *8*, 4588.
[28] C. Ziegler, *Ph.D. Thesis*, Technical University of Dresden, **2012**.
[29] T. Bayrak, S. Helmi, J. Ye, D. Kauert, J. Kelling, T. Schönherr, R. Weichelt, A. Erbe, R. Seidel, *Nano Lett.* **2018**, *18*, 2116.
[30] S. M. Douglas, A. H. Marblestone, S. Teerapittayanon, A. Vazquez, G. M. Church, W. M. Shih, *Nucleic Acids Res.* **2009**, *37*, 5001.
[31] Y. Ke, S. M. Douglas, M. Liu, J. Sharma, A. Cheng, A. Leung, Y. Liu, W. M. Shih, H. Yan, *J. Am. Chem. Soc.* **2009**, *131*, 15903.
[32] E. Stahl, T. G. Martin, F. Praetorius, H. Dietz, *Angew. Chem., Int. Ed.* **2014**, *53*, 12735.
[33] F. N. Gür, F. W. Schwarz, J. Ye, S. Diez, T. L. Schmidt, *ACS Nano* **2016**, *10*, 5374.
[34] S. Helmi, C. Ziegler, D. J. Kauert, R. Seidel, *Nano Lett.* **2014**, *14*, 6693.